Targeting integrin $\alpha_5\beta_1$ ameliorates severe airway hyperresponsiveness in experimental asthma

Aparna Sundaram,[1] Chun Chen,[1] Amin Khalifeh-Soltani,[2] Amha Atakilit,[1] Xin Ren,[1] Wenli Qiu,[1] Hyunil Jo,[3] William DeGrado,[3] Xiaozhu Huang,[1] and Dean Sheppard[1]

[1]Lung Biology Center, Department of Medicine, [2]Cardiovascular Research Institute, and [3]Department of Pharmaceutical Chemistry, UCSF, San Francisco, California, USA.

Treatment options are limited for severe asthma, and the need for additional therapies remains great. Previously, we demonstrated that integrin $\alpha_v\beta_6$-deficient mice are protected from airway hyperresponsiveness, due in part to increased expression of the murine ortholog of human chymase. Here, we determined that chymase protects against cytokine-enhanced bronchoconstriction by cleaving fibronectin to impair tension transmission in airway smooth muscle (ASM). Additionally, we identified a pathway that can be therapeutically targeted to mitigate the effects of airway hyperresponsiveness. Administration of chymase to human bronchial rings abrogated IL-13–enhanced contraction, and this effect was not due to alterations in calcium homeostasis or myosin light chain phosphorylation. Rather, chymase cleaved fibronectin, inhibited ASM adhesion, and attenuated focal adhesion phosphorylation. Disruption of integrin ligation with an RGD-containing peptide abrogated IL-13–enhanced contraction, with no further effect from chymase. We identified $\alpha_5\beta_1$ as the primary fibronectin-binding integrin in ASM, and $\alpha_5\beta_1$-specific blockade inhibited focal adhesion phosphorylation and IL-13–enhanced contraction, with no additional effect from chymase. Delivery of an $\alpha_5\beta_1$ inhibitor into murine airways abrogated the exaggerated bronchoconstriction induced by allergen sensitization and challenge. Finally, $\alpha_5\beta_1$ blockade enhanced the effect of the bronchodilator isoproterenol on airway relaxation. Our data identify the $\alpha_5\beta_1$ integrin as a potential therapeutic target to mitigate the severity of airway contraction in asthma.

Introduction

Severe asthma affects 5% to 10% of the total asthmatic population (1, 2). This subgroup is characterized by poor symptom control including persistent airflow obstruction and recurrent exacerbations, as well as frequent hospitalizations and high medication requirements, often with associated side effects, to control the disease (3, 4). Multiple studies have shown that patients with severe asthma have a poorer quality of life and increased financial costs as measured by increased days off work or school and increased health care utilization (3–6). Since the introduction of anti-IgE therapy in the early 2000s, the development of targeted immune therapies has grown at a meteoric pace. Unfortunately, current therapies targeting inflammatory mediators are only useful in a subset of patients with severe asthma (7–10). While prevention of asthma through these biologic strategies is undoubtedly important, the treatment of bronchoconstriction will always be required, and advances in therapeutics directly targeting smooth muscle have been notably lacking.

One of the consistent hallmarks of asthma is airway hyperresponsiveness, defined as exaggerated airway narrowing in response to a variety of stimuli (11, 12). We have previously shown that the murine mast cell protease 4 (mMCP-4) and its human ortholog, mast cell chymase, inhibit the exaggerated force generated by murine tracheal rings that have been incubated overnight with the asthmagenic inflammatory mediator IL-13 (13). Mice lacking mMCP-4 have also been shown to develop exaggerated airway hyperresponsiveness after allergen challenge (14), whereas mice lacking the $\alpha_v\beta_6$ integrin, which we have shown have markedly increased levels of mMCP-4 in intraepithelial mast cells, are protected from allergen-induced airway hyperresponsiveness (13). We therefore reasoned that elucidation of the mechanism(s) underlying these protective effects of mMCP-4 and chymase might lead to identification of new targets for the treatment of airway hyperresponsiveness in asthma.

We found that chymase protects against cytokine-enhanced contraction of murine and human airway smooth muscle (ASM) by cleavage of the extracellular matrix (ECM) protein fibronectin. This effect does not appear to be due to alteration of classic pathways regulating smooth muscle actin–myosin contraction, but is associated with a specific reduction in smooth muscle cell adhesion to fibronectin, a process mediated by the $\alpha_5\beta_1$ integrin. Notably, inhibition of this integrin by an antibody or small molecule mimics the protective effects of chymase on cytokine-enhanced force generation, and further addition of chymase has no additional effect. In vivo administration of a small-molecule inhibitor of $\alpha_5\beta_1$ directly into the airways of mice also inhibited the airway hyperresponsiveness induced by allergen sensitization and challenge. Finally, addition of an inhibitor of $\alpha_5\beta_1$ enhanced the bronchodilatory effect of the β-adrenergic agonist isoproterenol. These results underscore the idea that blunting the mechanical transmission of tension from smooth muscle to the surrounding ECM has functional consequences on the

Conflict of interest: The authors have declared that no conflict of interest exists.
Submitted: May 24, 2016; **Accepted:** October 27, 2016.
Reference information: *J Clin Invest*. 2017;127(1):365–374. doi:10.1172/JCI88555.

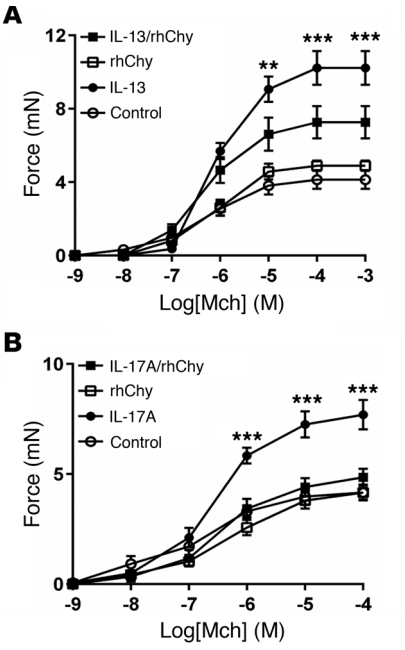

Figure 1. Chymase abrogates cytokine-enhanced airway contraction. (**A**) Force exerted on human bronchial rings measured after incubation for 12 hours in DMEM with IL-13 (100 ng/ml) or saline (control), then for 20 minutes with rhChy (30 nM) or vehicle, in response to a range of concentrations agonist Mch. n = 3–9 rings per group. $^{**}P < 0.01$ and $^{***}P < 0.001$, for IL-13 versus IL-13/rhChy; repeated measures of variance. (**B**) Contractile force of mouse tracheal rings measured after incubation for 12 hours in DMEM with IL-17A (100 ng/ml) or saline (control), then for 20 minutes with rhChy (30 nM) or vehicle in response to a range of concentrations of the contractile agonist Mch. n = 4–5 rings per group. $^{***}P < 0.001$, for IL-17A versus IL-17A/rhChy; repeated measures of variance. All data represent the mean ± SEM.

mechanics of airway narrowing. Our results also identify the $\alpha_5\beta_1$ integrin as a new target for treatment of the exaggerated airway narrowing that characterizes asthma.

Results

Recombinant human chymase protects against IL-13–enhanced contraction without modulating the classical actin/myosin pathway. Contractile responses to methacholine (Mch) were evaluated in human bronchial rings that were incubated with IL-13 (or vehicle) for 12 hours and treated with human chymase (or vehicle) for 20 minutes. Recombinant human chymase (rhChy) had no effect on the contraction of control bronchial rings but inhibited IL-13–enhanced contraction (Figure 1A), as we previously reported for contraction of mouse tracheal rings (13). This protective effect was also observed when rings were treated with IL-17A, suggesting that the mechanisms responsible for this effect are not cytokine specific and probably involve a common downstream pathway (Figure 1B).

We have previously shown that mMCP-4, the closest ortholog of human mast cell chymase, acts independently of the epithelium to directly modulate smooth muscle contraction (13). We therefore explored the effect of rhChy on the classical intracellular pathways in smooth muscle cells that contribute to contraction (Supplemental Figure 1A; supplemental material available online with this article; doi:10.1172/JCI88555DS1). Stimulation of smooth muscle cells by agonists such as KCl or Mch induce a rise in intracellular calcium concentration either through influx of extracellular calcium or the release of intracellular calcium from the sarcoplasmic reticulum (15). This transient increase in intracellular calcium activates downstream pathways to increase myosin light chain kinase activity and phosphorylate the myosin light chain, thus promoting actin-myosin coupling and smooth muscle contraction. The magnitude of contraction downstream of these transient increases in intracellular calcium is most highly correlated with the frequency of calcium oscillations rather than the magnitude of the individual increases (16–18). We thus measured the difference in frequency of Mch-induced calcium oscillations in mouse lung slices pretreated with IL-13 before and after treatment with rhChy and found no effect of chymase on calcium oscillations (Supplemental Figure 1B). The small guanosine triphosphatase (GTPase) RhoA can also contribute to the regulation of smooth muscle contraction through a calcium-independent pathway via inhibition of myosin light chain phosphatase. We therefore evaluated the effects of human chymase on RhoA activity, before and after treatment of both tracheal rings and human ASM cells with IL-13. As expected, IL-13 increased RhoA activity, but human chymase did not modulate this effect (Supplemental Figure 1C and Supplemental Figure 2A). Finally, we examined the effects of human chymase on phosphorylation of myosin light chain and myosin light chain phosphatase (Supplemental Figure 1D and Supplemental Figure 2B). Again, while IL-13 induced the expected increases in phosphorylation of each target in response to Mch, human chymase did not modulate these effects. Taken together, our data suggest that the mechanism for chymase-mediated protection from cytokine-enhanced contraction is unlikely to be related to modulation of the classical actin/myosin contraction pathway.

rhChy modulates the interaction of smooth muscle cells with the ECM protein fibronectin. In addition to activation of the actin-myosin power stroke cycle, generation of tension by ASM depends on firm adhesion of the muscle to the underlying ECM (19, 20). Mechanical force can regulate actin polymerization, stimulate the recruitment of the cytoskeletal linker and the signaling proteins focal adhesion kinase (FAK), paxillin, talin, vinculin, and α-actinin, and strengthen connections between these cytoskeletal adhesion complexes, integrins, and the ECM (21–25) (Figure 2A).

Histologic studies of asthmatic airways show altered profiles of ECM proteins including increased levels of collagens I, III, and V as well as fibronectin and laminin (26–28). We theorized that, since human mast cell chymase is released into the extracellular space, it may act on ECM proteins to modulate their interaction with smooth muscle cells. We directly examined the effect of chymase on cellular adhesion by treating ECM proteins with rhChy and measuring the resultant adhesion of human ASM cells. Treatment of fibronectin with chymase resulted in a dose-dependent decrease in adhesion (Figure 2B). We determined that the reduction in adhesion was due to direct effects of chymase on fibronectin and not to indirect effects on ASM cells themselves, since treatment of human ASM cells with chymase prior to incubation of these cells with fibronectin did not alter adhesion (Figure 2B).

We next sought to determine whether the effects of chymase were specific to fibronectin by examining the effects of chymase

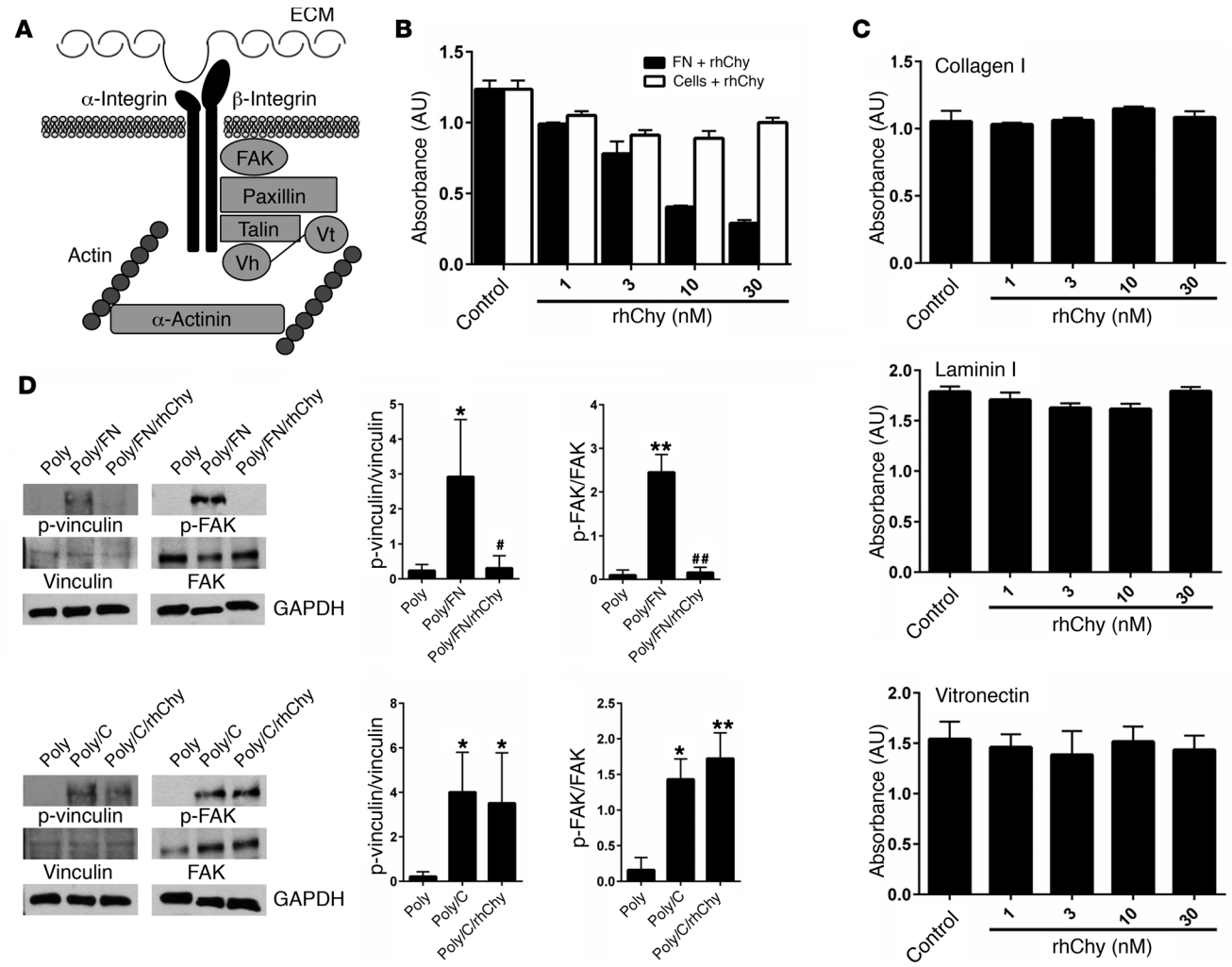

Figure 2. Chymase impairs smooth muscle adhesion to fibronectin and focal adhesion complex phosphorylation. (**A**) Schematic of alternate pathways important in the transmission of tension. Vh, vinculin head domain; Vt, vinculin tail domain. (**B**) Adhesion of human ASM cells to fibronectin measured by absorbance of crystal violet at 595 nm. Fibronectin (0.1 μg/ml) or cells were treated with the indicated doses of rhChy for 20 minutes and then chymostatin (10 μg/ml) prior to assessment of adhesion. (**C**) Adhesion of human ASM cells to collagen I (0.1 μg/ml), vitronectin (0.3 μg/ml), or laminin I (10 μg/ml), as measured by absorbance of crystal violet at 595 nm. Ligands were treated with the indicated doses of rhChy for 20 minutes and then chymostatin (10 μg/ml) prior to assessment of adhesion. (**B** and **C**) Data represent the mean ± SEM from triplicate experiments. (**D**) Representative Western blots and quantitative densitometry for phosphorylated and total vinculin and FAK in human ASM cells plated on poly-L-lysine (300 μg/ml) alone or poly-L-lysine with either fibronectin (1 μg/ml) or collagen I (1 μg/ml), with the addition of rhChy (30 nM) or vehicle for 20 minutes, followed by chymostatin (10 μg/ml). GAPDH was used as a loading control. Poly, poly-L-lysine; FN, fibronectin; C, collagen I. $^{*}P < 0.05$ and $^{**}P < 0.01$ versus Poly; $^{\#}P < 0.05$ and $^{\#\#}P < 0.01$ versus Poly/FN by 2-way ANOVA. $n = 3$ distinct experiments.

on ASM cell adhesion to alternative ECM proteins such as collagen I and laminin I. Chymase had no effect on adhesion to collagen I or laminin I (Figure 2C). Cellular adhesion to fibronectin is mediated in part by interactions between cell-surface integrins and a linear tripeptide sequence in the tenth fibronectin type III repeat, arginine-glycine–aspartic acid (RGD) (29). To determine whether chymase treatment might disrupt interactions with any RGD-containing integrin ligands, we also examined the effects of chymase on adhesion to vitronectin and again found no effect (Figure 2C). We further examined the effects of treatment with chymase on downstream signals induced by integrin ligation, specifically phosphorylation of the intracellular adhesion complex proteins vinculin and FAK. Adhesion to fibronectin or collagen induced phosphorylation of both downstream targets in human ASM cells compared with adhesion to poly-L-lysine (integrin-independent adhesion). These effects were inhibited by treatment of fibronectin with human chymase, but chymase treatment of collagen I had no effect on phosphorylation of either of these proteins (Figure 2D).

Chymase is an S1 serine protease and has been previously reported to have proteolytic activity against fibronectin (30, 31). We theorized that chymase may cleave fibronectin to interfere with the appropriate presentation of integrin recognition sites. We confirmed by Coomassie staining that chymase cleaves purified fibronectin in vitro (Figure 3A). A limited number of cleaved fibronectin fragments were also identified by Western blotting using a polyclonal antibody (Figure 3A), and cleavage was confirmed after ex vivo treatment of mouse tracheal strips with chymase (Figure 3B). We were unable to detect the major, smaller cleavage products by Western blotting,

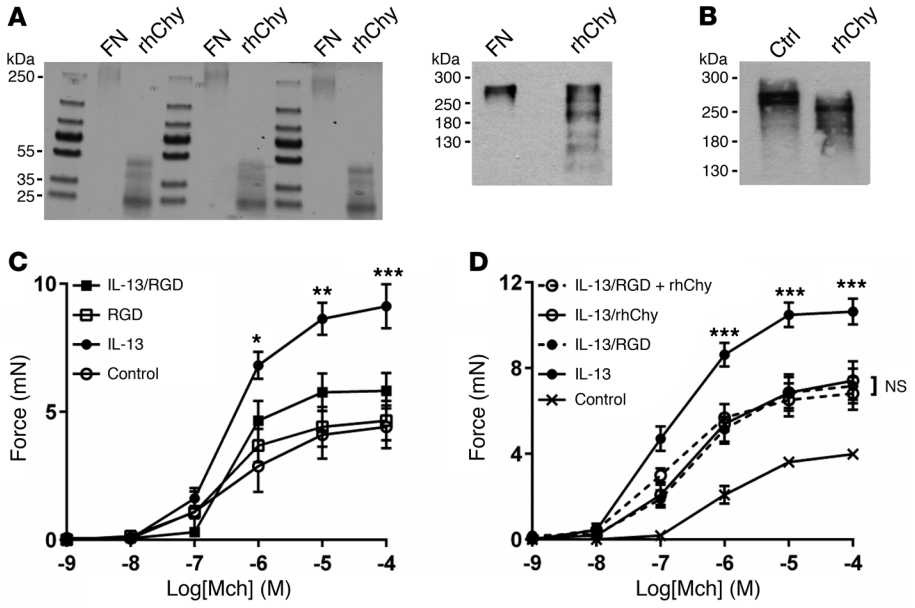

Figure 3. Chymase cleaves fibronectin and disrupts integrin binding to abrogate IL-13–enhanced contraction. (**A**) Coomassie staining (5 μg, left) and representative Western blot (50 μg, right) for fibronectin cleavage products in human plasma fibronectin after treatment with rhChy (30 nM) or vehicle for 20 minutes. (**B**) Representative Western blot for fibronectin cleavage products in mouse posterior tracheal smooth muscle strips after treatment with rhChy (30 nM) or vehicle for 20 minutes. Ctrl, control. (**C**) Contractile force of mouse tracheal rings measured after incubation for 12 hours in DMEM with IL-13 (100 ng/ml) or saline (control), then for 1 hour with GRGDSP peptide (RGD, 10 μg/ml) or vehicle in response to a range of concentrations of the contractile agonist Mch. $^{*}P < 0.05$, $^{**}P < 0.01$, and $^{***}P < 0.001$, for IL-13 versus IL-13/RGD; repeated measures of variance. (**D**) Contractile force of mouse tracheal rings measured after incubation for 12 hours in DMEM with IL-13 (100 ng/ml) or saline (control), then for 1 hour with GRGDSP (10 μg/ml), 20 minutes with rhChy (30 nM), or both, in response to a range of concentrations of Mch. $^{***}P < 0.001$, for IL-13 versus IL-13/RGD plus rhChy. NS, for IL-13/RGD versus IL-13/rhChy versus IL-13/RGD plus rhChy; repeated measures of variance. All data represent the mean ± SEM. n = 4–5 rings per group.

presumably because the epitopes recognized by the antibody we used were destroyed by one or more cleavage events.

To determine the functional effect of integrin ligation on the transmission of tension, we incubated tracheal rings with GRGDSP, an RGD-containing peptide derived from the tenth fibronectin type III repeat in fibronectin. We found that treatment with GRGDSP abrogated IL-13–enhanced contraction (Figure 3C). Furthermore, the addition of chymase to rings treated with GRGDSP did not confer additional protection from IL-13–enhanced contraction compared with treatment with either GRGDSP or chymase alone (Figure 3D), suggesting that GRGDSP and chymase act along the same pathway to inhibit integrin-mediated transmission of tension.

Integrin $\alpha_5\beta_1$ is critical for fibronectin-mediated adhesion and effective transmission of tension in smooth muscle. Integrins are heterodimeric proteins composed of one α and one β subunit (32). Although RGD has been identified as a general integrin-binding motif recognized by 8 of 24 mammalian integrins, individual integrins differentially bind to RGD sequences in the context of particular protein ligands or to more than one site in a single ligand. To further delineate the integrin(s) most relevant to fibronectin-mediated adhesion of human ASM cells, we first used flow cytometry to determine the potential fibronectin-binding integrins present on these cells. Using the promiscuous β_1 and α_v integrin subunits as positive controls and β_6 (present only on epithelial cells) as a negative control, we determined that integrins $\alpha_v\beta_3$, $\alpha_v\beta_5$, $\alpha_8\beta_1$, and $\alpha_5\beta_1$ were expressed (Figure 4A). There is currently no antibody specific for $\alpha_v\beta_1$, so we used IP, followed by Western blotting, to verify that $\alpha_v\beta_1$ was also expressed (Figure 4B). To address the possible confounder that either treatment with chymase or IL-13 could modulate integrin expression, we performed flow cytometry and found that there was no change in integrin expression at the cell surface after treatment with either chymase or IL-13 (Supplemental Figure 3, A and B). We also evaluated the effect of IL-13 on fibronectin expression and found no major differences in protein or mRNA expression within the cell or in secreted fibronectin in the media (Supplemental Figure 4, A and B). To determine the primary integrin(s) responsible for fibronectin-mediated adhesion, we performed cell adhesion assays with human ASM cells in the presence or absence of a variety of anti-integrin antibodies. Blockade of either the β_1 or α_5 subunit nearly completely inhibited adhesion to fibronectin, while blockade of β_3, β_5, α_v, and α_8 integrins had no effect on adhesion (Figure 4C), suggesting that integrin $\alpha_5\beta_1$ is the principal integrin mediating adhesion of ASM cells to fibronectin.

Integrin $\alpha_5\beta_1$ binds to the RGD sequence in the tenth fibronectin type III repeat with more affinity than do other integrins due to the presence of a PHSRN synergy region located in the ninth fibronectin type III repeat. This region is thought to have no adhesive activity by itself, but causes an increase of approximately 100-fold in the affinity of $\alpha_5\beta_1$ for fibronectin (33–35). We hypothesized that disruption of this interaction might explain the effect of chymase on inhibiting fibronectin-mediated adhesion. We performed N-terminal sequencing of the 3 major cleaved fibronectin bands identified in Figure 3A and identified a total of 5 cleavage sites within fibronectin. Three of the cleavage sites were in domains involved with fibrillogenesis, but, importantly, one cleavage site was within the tenth type III repeat between the PHSRN and RGD sequences (Figure 4D).

To investigate whether the loss of tethering of smooth muscle through the single integrin $\alpha_5\beta_1$ could have signaling effects, we showed that, as with chymase, blockade of integrin $\alpha_5\beta_1$ specifically inhibited phosphorylation of the intracellular adhesion complex proteins vinculin and FAK in ASM cells plated on fibronectin but not collagen I (Figure 5A). Prior to determining the functional consequences of blockade of $\alpha_5\beta_1$ on force generation, we identified that in human bronchial rings, integrin $\alpha_5\beta_1$ is most highly expressed in ASM, with relatively little expression in the subepithelial connective tissue and no expression in the airway epithelium (Supplemental Figure 5). We then examined

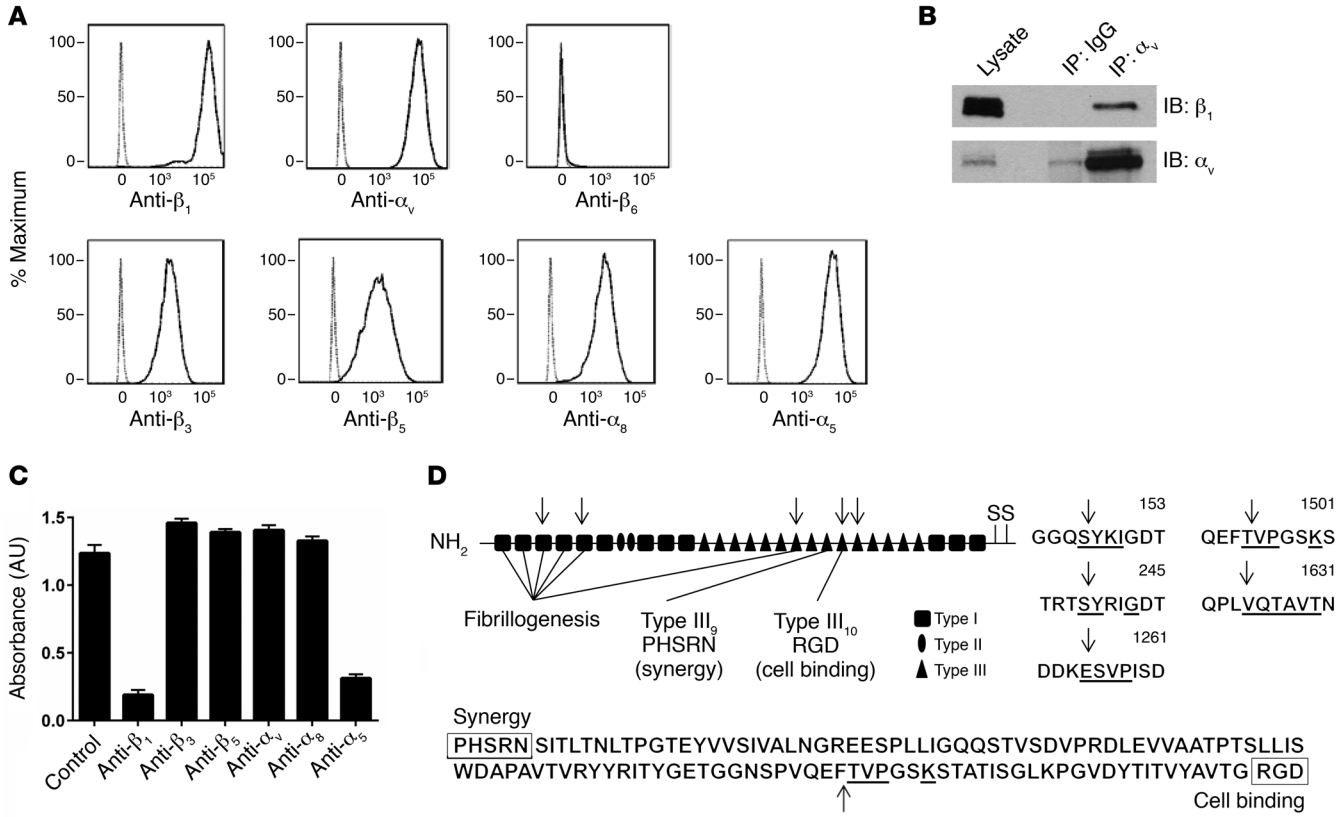

Figure 4. Integrin $\alpha_5\beta_1$ is critical for smooth muscle cell adhesion to fibronectin. (**A**) Human ASM cells in suspension were labeled with primary antibodies specific for cell-surface integrins β_1, α_v, β_6, β_3, β_5, α_8, α_5 and a secondary antibody conjugated to APC. The cells were analyzed by flow cytometry and gated for live cells. The resultant population was analyzed for APC expression (solid line). Human ASM cells labeled with a secondary antibody alone served as a control (dashed line). Representative histograms of APC expression versus cell counts are shown. The *x* axis represents APC expression (mean fluorescence intensity); the *y* axis represents the cell count (percentage of maximum). (**B**) Representative Western blot for expression of integrin $\alpha_v\beta_1$ was determined by IP. Lysates from human ASM cells underwent pulldown with mouse IgG or anti-α_v antibody, followed by immunoblotting (IB) for β_1. Immunoblotting for α_v was performed to confirm enrichment of α_v. $n = 3$ distinct experiments. (**C**) Adhesion (measured by absorbance of crystal violet at 595 nm) of human ASM cells to fibronectin (0.1 μg/ml) after treatment with the indicated specific integrin-blocking antibodies. Data represent the mean ± SEM from triplicate experiments. (**D**) Schematic of fibronectin, with arrows marking chymase cleavage sites identified during N-terminal sequencing of the 3 cleaved fibronectin bands seen on the Coomassie staining in Figure 3A. The underlined amino acids correspond to aligned sequences detected during N-terminal sequencing.

the effect of blockade of $\alpha_5\beta_1$ on tracheal rings using a blocking antibody directed against the α_5 subunit. This blocking antibody inhibited IL-13–enhanced contraction, but the effects were smaller than those we observed after treatment with chymase (Figure 5B). Given the difficulty of adequate antibody penetration into tracheal rings, we also tested the small-molecule inhibitor ATN-161, a 5-mer capped peptide derived from the PHSRN synergy region of fibronectin. As no other fibronectin-binding integrin requires this synergy site, ATN-161 has been proposed to interact primarily with $\alpha_5\beta_1$, though it has been shown to interact with other integrins including $\alpha_v\beta_3$ in vitro (36–38). Treatment with ATN-161 abrogated IL-13–enhanced contraction (Figure 5C) to a degree similar to that seen with human chymase, and, furthermore, the addition of chymase to rings treated with ATN-161 did not confer any additional protection compared with treatment with either ATN-161 or chymase alone (Figure 5D).

Integrin $\alpha_5\beta_1$ is a therapeutic target for the treatment of airway contraction. To determine the in vivo effect of inhibition of $\alpha_5\beta_1$ on airway hyperresponsiveness, we sensitized WT C57BL/6 mice with 3 weekly i.p. injections of OVA, followed by 3 consecutive days of i.n. challenge with OVA. We delivered ATN-161 i.n. 1 hour prior to measurement of airway responsiveness to acetylcholine and found that inhibition of $\alpha_5\beta_1$ protected against increased airway hyperresponsiveness after OVA challenge (Figure 6A). Differential counting of cells obtained by bronchoalveolar lavage revealed similar numbers of macrophages, eosinophils, lymphocytes, and neutrophils in the 2 groups (Supplemental Figure 6); H&E staining of lung sections revealed no differences in inflammation; and period acid-Schiff (PAS) staining of lung sections showed no differences in mucus staining (data not shown). To test the hypothesis that airway relaxation could be enhanced by targeting both the classical pathway involved in tension generation and the alternate pathway involved in transmission of tension to the ECM, mouse tracheal rings were treated with IL-13 and precontracted with a submaximal dose of Mch, and then relaxation responses to isoproterenol were evaluated after the addition of ATN-161 or vehicle. As expected, the addition of ATN-161 enhanced the relaxation induced by isoproterenol to near baseline (Figure 6B). Taken together, these data support the hypothesis that disruption of integrin-ECM association impairs the mechanical transmission of tension and identify integrin $\alpha_5\beta_1$ as a useful adjunctive therapeutic target for the treatment of airway hyperresponsiveness and bronchoconstriction in asthma.

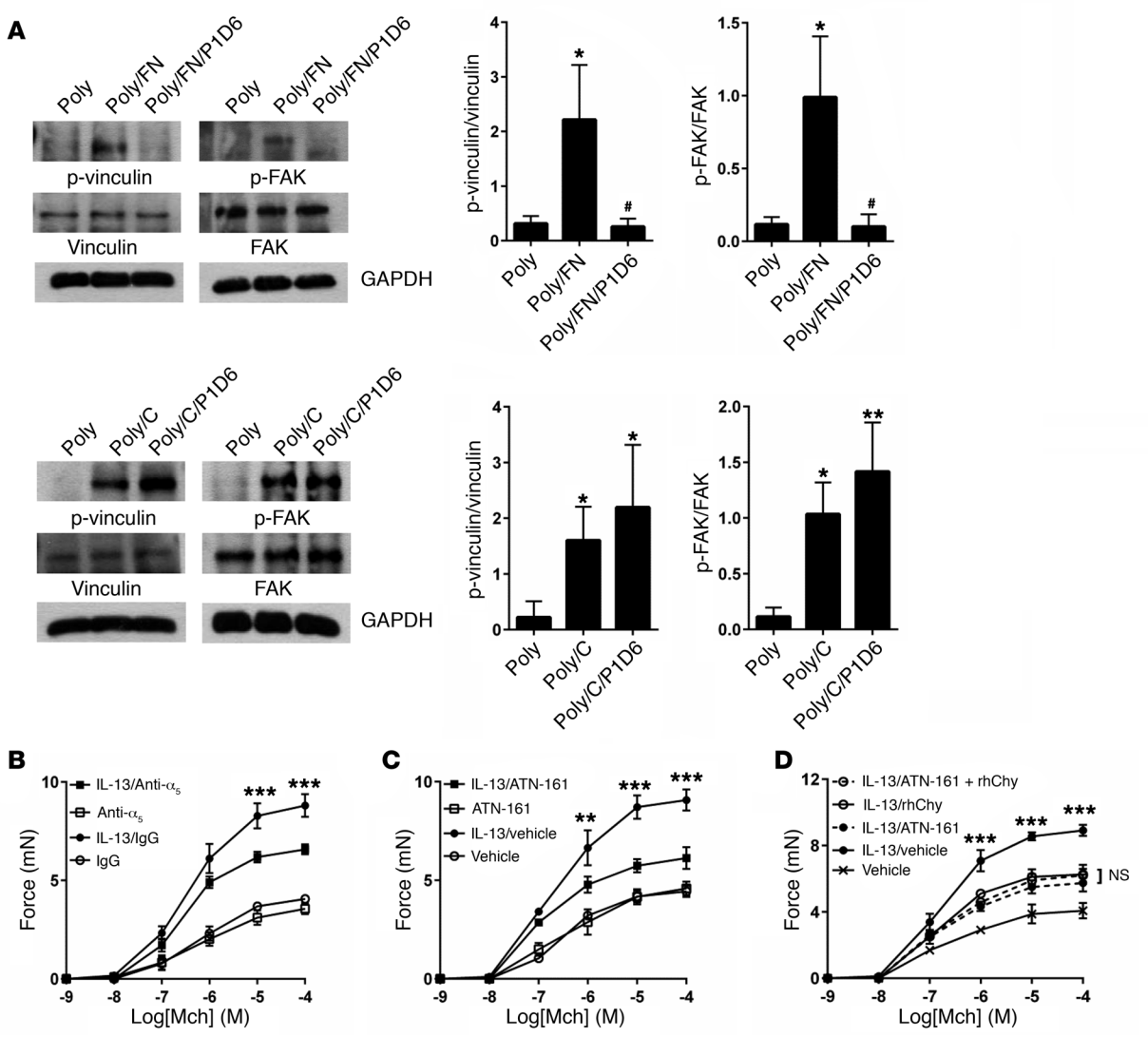

Figure 5. Blockade of $\alpha_5\beta_1$ inhibits focal adhesion phosphorylation and impairs IL-13–enhanced tracheal ring contraction. (**A**) Representative Western blot and quantitative densitometry for phosphorylated and total vinculin and FAK in human ASM cells treated for 20 minutes with integrin α_5–blocking antibody (P1D6, 10 μg/ml) or mouse IgG control, then plated on poly-L-lysine (300 μg/ml) or poly-L-lysine with either fibronectin (1 μg/ml) or collagen I (1 μg/ml). GAPDH was used as a loading control. $^*P < 0.05$ and $^{**}P < 0.01$ versus Poly; $^{\#}P < 0.05$ versus Poly/FN. $n = 3$ distinct experiments. GAPDH was used as a loading control. $^*P < 0.05$ and $^{**}P < 0.01$ versus Poly; $^{\#}P < 0.05$ versus Poly/FN, by 2-way ANOVA $n = 3$ distinct experiments. Data represent the mean ± SEM. (**B**) Contractile force of mouse tracheal rings measured after incubation for 12 hours in DMEM with IL-13 (100 ng/ml) or saline and for 12 hours with α_5-blocking antibody (300 μg/ml) or rat IgG in response to a range of concentrations of the contractile agonist Mch. $^{***}P < 0.001$, for IL-13/IgG versus IL-13/anti-α_5. (**C**) Contractile force of mouse tracheal rings measured after incubation for 12 hours in DMEM with IL-13 (100 ng/ml) or saline, then for 1 hour with a small-molecule inhibitor directed against the $\alpha_5\beta_1$ synergy site of fibronectin (ATN-161, 100 μg/ml) or vehicle in response to a range of concentrations of Mch. $^{**}P < 0.01$ and $^{***}P < 0.001$, for IL-13/vehicle versus IL-13/ATN-161. (**D**) Contractile force of mouse tracheal rings measured after incubation for 12 hours in DMEM with IL-13 (100 ng/ml) or saline (control), then for 1 hour with ATN-161 (100 μg/ml), 20 minutes with rhChy (30 nM), or both, in response to a range of concentrations of Mch. $^{***}P < 0.001$, for IL-13/vehicle versus IL-13/ATN-161 plus rhChy. NS, for IL-13/ATN-161 versus IL-13/rhChy versus IL-13/ATN-161 plus rhChy. (**B**–**D**) Data represent the mean ± SEM; n = 3–5 rings per group; significance was determined by repeated measures of variance.

Discussion

In the present study, we demonstrate that human chymase protects against the exaggerated generation of force by ASM induced by disease-relevant cytokines by cleaving extracellular fibronectin and impairing the interaction between extracellular fibronectin and the integrin $\alpha_5\beta_1$. Chymase and its ortholog murine mMCP-4 have previously been shown to have protective effects on exaggerated airway contraction (13). We have shown that the effects of mMCP-4 persist after removal of the airway epithelium, suggesting that its effects are likely to be on smooth muscle or the surrounding matrix. However, it was difficult to identify the mechanism for this protection, since chymase has been reported to affect a number of relevant biological processes by regulating mediators including angiotensin I (39–41), IL-1β (42), endothelin-1 (43), and TGF-β (44), as well as by modulating ECM components by cleaving pro-collagen Iα and fibronectin (31, 45). In this context, our observation that the effect of short-term exposure to chymase appears to be due to specific disruption of the interaction of a sin-

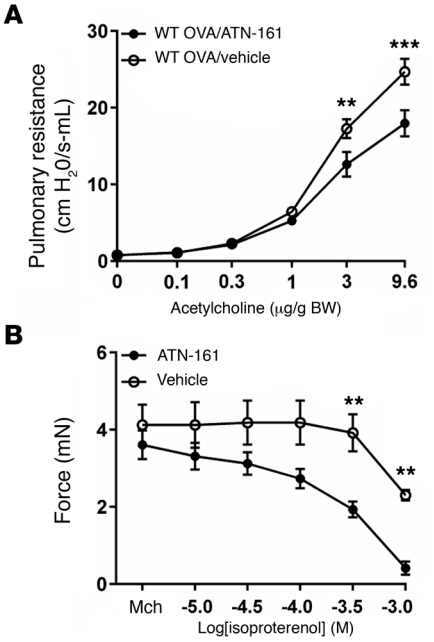

Figure 6. Inhibition of $\alpha_5\beta_1$ protects against airway hyperresponsiveness and enhances the effect of bronchodilators. (**A**) Pulmonary resistance measurements in WT C57Bl/6 mice following immunization and i.n. challenge with OVA, with i.n. administration of ATN-161 (12.5 mg/kg) or vehicle (5% DMSO, 0.9% saline) 1 hour prior to measurements. n = 8 animals per group. (**B**) Tension of mouse tracheal rings measured after 12 hours in DMEM with IL-13 (100 ng/ml) and incubation for 15 minutes with Mch (10^{-6} M) in response to a range of concentrations of the β-adrenergic agonist isoproterenol in the presence of ATN-161 (100 μg/ml) or vehicle. n = 5–8 rings per group. Data represent the mean ± SEM. $^{**}P < 0.01$ and $^{***}P < 0.001$; repeated measures of variance.

gle ECM protein, fibronectin, with a single integrin, $\alpha_5\beta_1$, makes this problem more tractable.

More importantly, the finding that ligation of the $\alpha_5\beta_1$ integrin has functional consequences for the exaggerated generation of force by ASM is, in our view, a significant discovery. Traditional models for the regulation of smooth muscle contraction have centered on pathways affecting actin-myosin cross-bridge interactions. However, there is growing evidence that contractile or mechanical stimuli also initiate other independently regulated cellular processes including focal adhesion assembly, actin filament polymerization, and cytoskeletal network stabilization (21–25). These pathways provide a rigid network connecting intracellular actin filaments to the ECM to allow for effective transmission of force throughout the smooth muscle (19, 20). Our findings that disruption of this connection impairs tension development underscore the importance of these complex cytoskeletal events in force generation and can be leveraged therapeutically in the treatment of bronchoconstriction.

Most of the recent clinical trials for novel therapeutics in asthma have focused on cytokine signaling or immune biology and have included inhibitors of IgE, IL-5, IL-13, and IL-17, among others (7–10). Meanwhile, drugs targeting ASM function have been far fewer in number and have met with little success to date, in part because intracellular signaling converges on a singular signaling pathway, and calcium homeostatic pathways are integral to most cell types. In this context, our finding that integrin ligation mitigates force generation in ASM by impairing the extracellular mechanical transmission of tension without altering intracellular signaling is especially important, because it suggests a novel strategy for treating bronchoconstriction that works through a parallel pathway independently from the interventions reported to date.

Targeting the $\alpha_5\beta_1$ integrin would be expected to augment the effects of existing therapies (such as β-adrenergic agonists or muscarinic antagonists) and dampen exaggerated airway responsiveness, even under circumstances in which existing interventions are ineffective. Currently available inhibitors of $\alpha_5\beta_1$, including ATN-161, are limited in their potency and specificity. Although multiple inhibitors of the $\alpha_5\beta_1$ integrin have been shown to be safe in preclinical animal studies, specificity for $\alpha_5\beta_1$ over other RGD-binding integrins remains an elusive target, in part because several of these inhibitors were developed as anticancer agents, in which multi-integrin antagonism has been more effective in animal models of tumor invasion. Nevertheless, the inhibitors currently being used in active clinical trials, including ATN-161, do not have significant reported toxicity (46, 47), suggesting that new drugs targeting this pathway could be rapidly moved into clinical trials for intervention in asthma.

One curious aspect of the results we describe is that all of our interventions (chymase, GRGDSP, and $\alpha_5\beta_1$ integrin inhibition) only affected the force generation of airway rings pretreated with asthmagenic cytokines (IL-13 or IL-17A) but did not affect the baseline force generated by the untreated airway rings. One might have imagined that the ability to transmit force between integrins and the underlying ECM would also be important for force generation in normal, untreated airways. However, fibronectin is not the only matrix protein present around ASM in vivo, so we did not expect that cleavage of fibronectin would completely abrogate the ability of contracting ASM to generate force. We interpret our results as evidence that the specific interaction between $\alpha_5\beta_1$ integrin and fibronectin is only needed to sustain the exaggerated force generated by ASM in pathologic conditions, as mimicked by incubation with the disease-relevant cytokines IL-13 and IL-17A. Such a differential effect on enhanced, but not baseline, contraction is not without precedent. For example, it was recently shown that the secreted adaptor protein milk fat globule–EGF factor 8 (MFG-E8) is important for the prevention of exaggerated force generation in airway rings pretreated with IL-13 but has no effect on force generation in untreated rings (48). Indeed, the specificity of the effects of $\alpha_5\beta_1$ inhibition on pathologic force generation, with no effect on normal homeostatic contraction, makes it an even more attractive target for therapeutic intervention.

In summary, we found that human chymase inhibits pathologic force generation by ASM by cleaving the ECM protein fibronectin and specifically inhibiting the interaction between fibronectin and the integrin $\alpha_5\beta_1$ expressed on ASM. This effect does not alter the classic pathways regulating actin-myosin contraction but does inhibit phosphorylation of integrin signaling and adaptor proteins that have been shown to be important for the transmission of force from integrins to their ECM ligands. These findings help explain why mice lacking the closest ortholog of human chymase develop exaggerated airway hyperresponsiveness induced by allergic sensitization and challenge (14) and why chymase expression has been associated with reduced severity of human asthma (49). More important, we believe that these

findings identify integrin $\alpha_5\beta_1$ as a novel therapeutic target to enhance the effect of currently available bronchodilator therapy for asthma.

Methods

Reagents. Rabbit phosphorylated myosin light chain (p–myosin light chain), myosin light chain, p–myosin phosphatase, myosin phosphatase, vinculin, FAK, and GAPDH antibodies were purchased from Cell Signaling Technology. Mouse RhoA antibody was purchased from Cytoskeleton. Rabbit integrin β_1 and p-vinculin antibodies were purchased from EMD Millipore. Mouse integrin α_v antibody was purchased from BD Biosciences. Rabbit fibronectin and p-FAK antibodies were purchased from Abcam. Mouse IgG and rat IgG were purchased from Jackson ImmunoResearch. For immunostaining, rabbit anti–integrin α_5 was purchased from Abcam, and mouse anti–α–smooth muscle actin antibody (clone 1A4) was purchased from Sigma-Aldrich.

Cells. Human ASM cells and media were purchased from Lonza and cultured according to the manufacturer's instructions. Cells were used between passages 5 and 10.

Mice. Six- to ten-week-old C57BL/6 mice were used for all experiments and were housed under specific pathogen–free conditions in the Animal Barrier Facility at UCSF. Sex-matched littermate controls were used in all experiments for tracheal ring contractility, lung slice calcium oscillation, and airway hyperresponsiveness.

Murine models of allergic airway disease. Six-week-old, sex-matched C57/Bl6 mice were sensitized on days 0, 7, and 14 by i.p. injection of 50 μg OVA (Sigma-Aldrich) emulsified in 1 mg aluminum potassium sulfate. Subsequently, mice were anesthetized with isoflurane and i.n. challenged on 3 consecutive days (days 21, 22, and 23) by aspiration of 100 μg OVA dissolved in 40 μl saline. Twenty-four hours after the last challenge, mice were anesthetized with isoflurane and underwent computer-generated randomization to be given either ATN-161 (12.5 mg/kg in 5% DMSO, 0.9% sodium chloride) or vehicle (5% DMSO, 0.9% sodium chloride) i.n. One hour after administration, mice were anesthetized with ketamine (100 mg/kg), xylazine (10 mg/kg), and acepromazine (3 mg/kg). Pulmonary resistance was determined using invasive cannulation of the trachea as previously described (50). The scientists performing the experiment were blinded to the drug delivered throughout the experiment and during analysis of the experimental outcome.

Assessment of pulmonary inflammation and mucus production. Lungs were subjected to 5 consecutive lavages with 0.8 ml PBS. After lysing red blood cells, the total cells were counted with a hemocytometer. Cytospin preparations were stained with a HEMA 3 Stain Set (Thermo Fisher Scientific), and cell differential percentages were determined on the basis of light microscopic evaluation of more than 300 cells per slide. Lavaged lungs were inflated with 10% buffered formalin to 25 cm H_20 of pressure. Multiple paraffin-embedded 5-μm sections of the entire mouse lung were prepared and stained with H&E and PAS to evaluate mucus production.

Measurement of chymase activity. *N*-succinyl-Ala-Ala-Pro-Phe-*p*-nitroanilide (1 mM) (Suc-AAPF-pNA; Sigma-Aldrich) was stabilized in buffer (0.45 M Tris-HCl, pH 8.0, 1.8 M NaCl, 9% DMSO). rhChy (1 μl) (Sigma-Aldrich) was added, and absorbance was measured every second for 3 minutes at 410 nm with a standard 1-cm path-length cuvette at 37°C and then converted to a concentration of active enzyme.

Measurement of tracheal smooth muscle contractility. Tracheal ring contraction studies were performed as described previously (51). Briefly, after incubation with 30 nM rhChy for 20 minutes; 10 μg/ml GRGDSP peptide (Gibco, Thermo Fisher Scientific) for 1 hour; 300 μg/ml anti–integrin $\alpha_5\beta_1$ (BMB5; EMD Millipore) for 12 hours; and/or 100 μg/ml ATN-161 (MedKoo Biosciences) for 1 hour at 37°C with 5% CO_2, the rings were equilibrated under 0.5 gm of applied tension, contracted with 60 mM KCl, and only rings that generated more than 1 mN of force were analyzed. After reequilibration, contractile responses to increasing doses of Mch (Sigma-Aldrich) were evaluated. For analysis of the suppressive effects on IL-13– or IL-17A–induced contractility, rings were treated with mouse IL-13 or IL-17A (100 ng/ml) (Peprotech) for 12 hours at 37°C in 5% CO_2. For relaxation experiments, rings were treated with mouse IL-13 (100 ng/ml) for 12 hours at 37°C with 5% CO_2, then precontracted with 10^{-6} M Mch, and relaxation responses to increasing doses of isoproterenol (Sigma-Aldrich) in the presence of ATN-161 (100 μg/ml) or vehicle were evaluated. For human bronchial rings, human lung tissue was obtained from lung transplant donors. Bronchi, 5–8 mm in diameter, were dissected free of connective tissue and cut into 4-mm-thick rings. The rings were stored overnight at 37°C in 5% CO_2 in DMEM medium. Contraction was assessed as above, except a resting tension of 1 g was applied, the rings were first contracted with 120 mM KCl after equilibration for 2 hours, and only the rings that generated more than 2 mN tension were used for experiments. Rings were then washed and reequilibrated before contractile responses to increasing concentrations of Mch were evaluated.

Calcium oscillations in lung slices. Lung slices from 6- to 10-week-old mice were prepared as previously described (51). Briefly, lungs were inflated with 1.0 ml of 2% low-melt agarose at 37°C through a tracheal catheter, followed by 0.2 ml air to flush the agarose out of the airways. Lungs were cooled to 4°C and sectioned with a vibratome (EMS-4000; Electron Microscopy Sciences) into 140-μm sections. Slices were maintained in DMEM with antibiotics at 37°C in 10% CO_2 overnight with IL-13 (100 ng/ml) for 12 hours. Slices were loaded with Oregon Green 488 BAPTA-AM (Invitrogen) (20 μM in HBSS containing 0.1% pluronic F-127 and 100 μM sulfobromophthalein) for 45 minutes at 30°C and de-esterified for 30 minutes at 30°C in HBSS containing 100 μM sulfobromophthalein. Slices were treated for 20 minutes with rhChy (30 nM) or vehicle and a single dose of 10^{-4} M Mch. Fluorescence imaging was performed with a Nikon spinning-disk confocal microscope at 20 frames per second. Changes in fluorescence intensity from the selected regions of interest (5 × 5 pixels) were analyzed with ImageJ software (NIH).

Assessment of RhoA activation. The RhoA activation assay was performed according to the manufacturer's instructions (Cytoskeleton). Briefly, smooth muscle dissected from posterior mouse trachea or cultured cells were homogenized in lysis buffer (50 mM Tris-HCl, pH 7.5, 10 mM $MgCl_2$, 0.5 M NaCl, 1% Triton X-100, and protease and phosphatase inhibitor cocktail) (Thermo Fisher Scientific). The supernatants were collected after centrifugation and incubated with GST-rhotekin bound to glutathione-agarose beads at 4°C for 1 hour. The beads were washed with a washing buffer containing 25 mM Tris, pH 7.5, 30 mM $MgCl_2$, and 40 mM NaCl. GTP-bound RhoA was detected by immunoblotting. Equivalent volumes from total lysates for each sample were used as loading controls.

Immunoblotting. Smooth muscle dissected from mouse tracheas or cultured cells were homogenized in lysis buffer (50 mM Tris-HCl, pH 7.5, 10 mM $MgCl_2$, 150 mM NaCl, 1% Triton X-100, 10 mM NaF, 1 mM Na_3VO_4) with a protease and phosphatase inhib-

itor cocktail (Thermo Fisher Scientific). Lysates were centrifuged, and the supernatant was resolved by SDS-PAGE and transferred to a PVDF membrane (EMD Millipore). For fibronectin cleavage, purified human plasma fibronectin (Calbiochem) was treated with 30 nM of rhChy for 20 minutes and then resolved by SDS-PAGE, followed by either Coomassie staining or transfer to a membrane. Membranes were blocked for 1 hour with 5% skim milk or 5% BSA in TBS with Tween-20, incubated at room temperature for 2 hours with primary antibodies, washed in TBS with Tween-20, incubated for 1 hour with peroxidase-conjugated secondary antibody, washed in TBS with Tween-20, and developed with ECL Plus (PerkinElmer) prior to exposure to film (Denville Scientific). All quantitative densitometry was calculated using ImageJ software.

N-terminal sequencing. Purified human plasma fibronectin was treated with 30 nM rhChy for 20 minutes, then resolved by SDS-PAGE, followed by brief Coomassie staining. N-terminal sequencing and amino acid analysis were performed at the Molecular Structure Facility of UC Davis (Davis, California, USA).

IP. Human ASM cells were lysed in 1% Triton X-100, 25 mM Tris-HCl, 125 mM NaCl, 10 mM EDTA, and a protease and phosphatase inhibitor cocktail (Thermo Fisher Scientific) and incubated with integrin α_v antibody (L230; provided by the Sheppard laboratory) for 1 hour at 4°C with rotation (70 rpm). Protein G sepharose beads were then added, with a further incubation for 1 hour. Samples were washed 4 times with 1 ml lysis buffer and eluted with reducing sample buffer, resolved by SDS-PAGE, and analyzed by immunoblotting.

Immunostaining. Human bronchial rings were embedded in OCT, and 5-μm sections were prepared using a Leica Cryostat CM1850. The sections were fixed with 4% paraformaldehyde, permeabilized with 0.3% Triton X-100, blocked with 10% serum, and incubated with primary antibody overnight. This was followed by PBS washes, incubation with the appropriate secondary antibody for 1 hour, and PBS washes. Sections were mounted in mounting medium with DAPI and visualized with a Leica DM5000B epifluorescence microscope.

Flow cytometry. Human ASM cells were harvested with 10 mM EDTA, washed twice with PBS, and resuspended in FACS buffer (PBS supplemented with 10% serum and 1% BSA). Cells (5×10^5) were then incubated with a primary antibody at 4°C for 30 minutes in the dark. Cells were then washed, resuspended in FACS buffer, and incubated with a secondary antibody conjugated to allophycocyanin (APC) (Jackson ImmunoResearch). Cells were then washed, resuspended in 2.5% serum, and analyzed on a BD FACSCanto II flow cytometer. The following antibodies were used: 10 μg/ml mouse anti–integrin β_1 (P5D2); anti–integrin α_v (L230); anti–integrin β_6 (3G9); anti–integrin β_3 (Axum-2); anti–integrin β_5 (Alula) (all from the Sheppard laboratory); 2 μg/ml chicken anti–integrin α_8 (INY-13; a gift of Yasuyuki Yokasaki, National Hiroshima Hospital, Saijoh, Higashi-Hiroshima, Japan.); and 10 μg/ml anti–integrin α_5 (P1D6; Abcam).

Quantitative real-time PCR. Total RNA was isolated with an RNeasy Kit (QIAGEN). cDNA was analyzed by SYBR green quantitative real-time PCR with an ABI 7900HT thermocycler and normalized to *GAPDH* expression. The primers used were as follows: *GAPDH*, forward, GGAGCGAGATCCCTCCAAAAT; *GAPDH*, reverse, GGCTGTTGTCATACTTCTCATGG; and fibronectin, forward, CGGTGGCTGTCAGTCAAAG; fibronectin, reverse, AAACCTCGGCTTCCTCCATAA.

Cell adhesion assay. Ninety-six–well flat-bottomed tissue culture plates (Linbro) were coated with 0.1 μg/ml human plasma fibronectin (Sigma-Aldrich); 0.1 μg/ml rat tail collagen I (Sigma-Aldrich); 10 μg/ml laminin I (R&D Systems); or 0.3 μg/ml human plasma vitronectin (Sigma-Aldrich) for 1 hour at 37°C. For immunoblots, 10-cm petri dishes (Fisherbrand) were coated with 1 μg/ml fibronectin, 1 μg/ml collagen I, or 300 μg/ml poly-L-lysine (Sigma-Aldrich). After incubation, wells were washed with PBS, then blocked with 1% BSA at 37°C for 1 hour. Control wells were filled with 1% BSA. Human ASM cells were detached using 10 mM EDTA and resuspended in serum-free DMEM. For blocking experiments, cells were incubated with 10 μg/ml of the indicated antibody for 15 minutes at 4°C before plating. For chymase experiments, the ligand or cells were treated with the indicated dose of rhChy for 20 minutes (Figure 2, B and C). The chymase was then neutralized with 10 μg/ml chymostatin (Sigma-Aldrich). The plates were centrifuged at 10 *g* for 5 minutes before incubation for 1 hour at 37°C in humidified 5% CO_2. Nonadherent cells were removed by centrifugation (top side down) at 10 *g* for 5 minutes. Attached cells were homogenized in lysis buffer as described above for immunoblotting, or were stained with 0.5% crystal violet, and the wells were washed with PBS. The relative number of cells in each well was evaluated after solubilization in 40 μl of 2% Triton X-100 by measuring absorbance at 595 nm in a microplate reader (Bio-Rad). All determinations were carried out in triplicate.

Statistics. The statistical significance of differences between 2 groups was calculated with a 2-tailed Student's *t* test. Two-way ANOVA was used for comparisons within or between multiple groups, with repeated measures of variance for related samples, and when differences were statistically significant ($P \leq 0.05$), this was followed with a Tukey's *t* test for subsequent pairwise analysis. All calculations were performed using GraphPad Prism (GraphPad Software).

Study approval. All mice were housed in a specific pathogen–free animal facility at UCSF. Animals were treated according to protocols that were approved by the IACUC of UCSF, in accordance with NIH guidelines. For human bronchial ring contractility experiments, cadaveric human lungs were obtained from brain-dead donors whose lungs could not be used for transplantation and therefore did not require approval of the UCSF Committee on Human Research.

Author contributions

AS and DS designed the experiments and prepared the manuscript. AS, CC, AKS, AA, XR, and WQ performed the experiments. AS, CC, AK, XR, and XH collected and analyzed the data. AA, HJ, WD, and XH provided reagents, technical support, and conceptual advice.

Acknowledgments

We thank George Caughey (VA Medical Center, San Francisco, California, USA) and members of his laboratory for their technical advice. This work was supported by grants from the National Heart, Lung, and Blood Institute (NHLBI), NIH (F32 HL 112588-01, K08 HL 124049-01, to A. Sundaram); the National Institute of Allergy and Infectious Diseases (NIAID), NIH (U19 Early Stage Investigator grant AI 070412-09, to A. Sundaram); the NHLBI, NIH (HL 102292, to D. Sheppard); and the NIAID, NIH (U19 AI 077439, to D. Sheppard).

Address correspondence to: Aparna Sundaram, University of California, San Francisco, 1550 4th Street, Box 2922, San Francisco, California 94143-2922, USA. Phone: 415.514.4275; E-mail: aparna.sundaram@ucsf.edu.

1. Barnes PJ, Woolcock AJ. Difficult asthma. *Eur Respir J*. 1998;12(5):1209–1218.
2. Busse WW, Banks-Schlegel S, Wenzel SE. Pathophysiology of severe asthma. *J Allergy Clin Immunol*. 2000;106(6):1033–1042.
3. Juniper EF, Wisniewski ME, Cox FM, Emmett AH, Nielsen KE, O'Byrne PM. Relationship between quality of life and clinical status in asthma: a factor analysis. *Eur Respir J*. 2004;23(2):287–291.
4. Hartert TV, et al. Risk factors for recurrent asthma hospital visits and death among a population of indigent older adults with asthma. *Ann Allergy Asthma Immunol*. 2002;89(5):467–473.
5. Juniper EF. Effect of asthma on quality of life. *Can Respir J*. 1998;5(Suppl A):77A–84A.
6. Rabe KF, et al. Worldwide severity and control of asthma in children and adults: the global asthma insights and reality surveys. *J Allergy Clin Immunol*. 2004;114(1):40–47.
7. Busse WW, et al. Randomized, double-blind, placebo-controlled study of brodalumab, a human anti-IL-17 receptor monoclonal antibody, in moderate to severe asthma. *Am J Respir Crit Care Med*. 2013;188(11):1294–1302.
8. Hanania NA, et al. Exploring the effects of omalizumab in allergic asthma: an analysis of biomarkers in the EXTRA study. *Am J Respir Crit Care Med*. 2013;187(8):804–811.
9. Pavord ID, et al. Mepolizumab for severe eosinophilic asthma (DREAM): a multicentre, double-blind, placebo-controlled trial. *Lancet*. 2012;380(9842):651–659.
10. Corren J, et al. Lebrikizumab treatment in adults with asthma. *N Engl J Med*. 2011;365(12):1088–1098.
11. Hargreave FE, O'Byrne PM, Ramsdale EH. Mediators, airway responsiveness, and asthma. *J Allergy Clin Immunol*. 1985;76(2 Pt 2):272–276.
12. Postma DS, Kerstjens HA. Characteristics of airway hyperresponsiveness in asthma and chronic obstructive pulmonary disease. *Am J Respir Crit Care Med*. 1998;158(5 Pt 3):S187–S192.
13. Sugimoto K, et al. The αvβ6 integrin modulates airway hyperresponsiveness in mice by regulating intraepithelial mast cells. *J Clin Invest*. 2012;122(2):748–758.
14. Waern I, et al. Mouse mast cell protease 4 is the major chymase in murine airways and has a protective role in allergic airway inflammation. *J Immunol*. 2009;183(10):6369–6376.
15. Kannan MS, Prakash YS, Brenner T, Mickelson JR, Sieck GC. Role of ryanodine receptor channels in Ca2+ oscillations of porcine tracheal smooth muscle. *Am J Physiol*. 1997; 272(4 Pt 1):L659–L664.
16. Perez JF, Sanderson MJ. The contraction of smooth muscle cells of intrapulmonary arterioles is determined by the frequency of Ca2+ oscillations induced by 5-HT and KCl. *J Gen Physiol*. 2005;125(6):555–567.
17. Perez JF, Sanderson MJ. The frequency of calcium oscillations induced by 5-HT, ACH, and KCl determine the contraction of smooth muscle cells of intrapulmonary bronchioles. *J Gen Physiol*. 2005;125(6):535–553.
18. Prakash YS, Pabelick CM, Kannan MS, Sieck GC. Spatial and temporal aspects of ACh-induced [Ca2+]i oscillations in porcine tracheal smooth muscle. *Cell Calcium*. 2000;27(3):153–162.
19. Huang Y, Day RN, Gunst SJ. Vinculin phosphorylation at Tyr1065 regulates vinculin conformation and tension development in airway smooth muscle tissues. *J Biol Chem*. 2014;289(6):3677–3688.
20. Zhang W, Gunst SJ. Dynamic association between alpha-actinin and beta-integrin regulates contraction of canine tracheal smooth muscle. *J Physiol (Lond)*. 2006;572(Pt 3):659–676.
21. Gunst SJ, Zhang W. Actin cytoskeletal dynamics in smooth muscle: a new paradigm for the regulation of smooth muscle contraction. *Am J Physiol, Cell Physiol*. 2008;295(3):C576–C587.
22. Tang DD, Anfinogenova Y. Physiologic properties and regulation of the actin cytoskeleton in vascular smooth muscle. *J Cardiovasc Pharmacol Ther*. 2008;13(2):130–140.
23. Tang DD. p130 Crk-associated substrate (CAS) in vascular smooth muscle. *J Cardiovasc Pharmacol Ther*. 2009;14(2):89–98.
24. Gunst SJ, Tang DD. The contractile apparatus and mechanical properties of airway smooth muscle. *Eur Respir J*. 2000;15(3):600–616.
25. Burridge K, Chrzanowska-Wodnicka M. Focal adhesions, contractility, and signaling. *Annu Rev Cell Dev Biol*. 1996;12:463–518.
26. Roberts CR, Burke AK. Remodelling of the extracellular matrix in asthma: proteoglycan synthesis and degradation. *Can Respir J*. 1998;5(1):48–50.
27. Roche WR, Beasley R, Williams JH, Holgate ST. Subepithelial fibrosis in the bronchi of asthmatics. *Lancet*. 1989;1(8637):520–524.
28. Laitinen LA, et al. Bronchial biopsy findings in intermittent or "early" asthma. *J Allergy Clin Immunol*. 1996;98(5 Pt 2):S3–6; discussion S33.
29. Pierschbacher MD, Ruoslahti E. Cell attachment activity of fibronectin can be duplicated by small synthetic fragments of the molecule. *Nature*. 1984;309(5963):30–33.
30. Schechter NM. Human chymase. *Monogr Allergy*. 1990;27:114–131.
31. Tchougounova E, Forsberg E, Angelborg G, Kjéllen L, Pejler G. Altered processing of fibronectin in mice lacking heparin. a role for heparin-dependent mast cell chymase in fibronectin degradation. *J Biol Chem*. 2001;276(6):3772–3777.
32. Hynes RO. Integrins: bidirectional, allosteric signaling machines. *Cell*. 2002;110(6):673–687.
33. Obara M, Kang MS, Yamada KM. Site-directed mutagenesis of the cell-binding domain of human fibronectin: separable, synergistic sites mediate adhesive function. *Cell*. 1988;53(4):649–657.
34. Kimizuka F, et al. Role of type III homology repeats in cell adhesive function within the cell-binding domain of fibronectin. *J Biol Chem*. 1991;266(5):3045–3051.
35. Aota S, Nomizu M, Yamada KM. The short amino acid sequence Pro-His-Ser-Arg-Asn in human fibronectin enhances cell-adhesive function. *J Biol Chem*. 1994;269(40):24756–24761.
36. Mould AP, et al. Defining the topology of integrin alpha5beta1-fibronectin interactions using inhibitory anti-alpha5 and anti-beta1 monoclonal antibodies. Evidence that the synergy sequence of fibronectin is recognized by the amino-terminal repeats of the alpha5 subunit. *J Biol Chem*. 1997;272(28):17283–17292.
37. Danen EH, Aota S, van Kraats AA, Yamada KM, Ruiter DJ, van Muijen GN. Requirement for the synergy site for cell adhesion to fibronectin depends on the activation state of integrin alpha 5 beta 1. *J Biol Chem*. 1995;270(37):21612–21618.
38. Khalili P, et al. A non-RGD-based integrin binding peptide (ATN-161) blocks breast cancer growth and metastasis in vivo. *Mol Cancer Ther*. 2006;5(9):2271–2280.
39. Reilly CF, Tewksbury DA, Schechter NM, Travis J. Rapid conversion of angiotensin I to angiotensin II by neutrophil and mast cell proteinases. *J Biol Chem*. 1982;257(15):8619–8622.
40. Urata H, Kinoshita A, Misono KS, Bumpus FM, Husain A. Identification of a highly specific chymase as the major angiotensin II-forming enzyme in the human heart. *J Biol Chem*. 1990;265(36):22348–22357.
41. Wintroub BU, Schechter NB, Lazarus GS, Kaempfer CE, Schwartz LB. Angiotensin I conversion by human and rat chymotryptic proteinases. *J Invest Dermatol*. 1984;83(5):336–339.
42. Mizutani H, Schechter N, Lazarus G, Black RA, Kupper TS. Rapid and specific conversion of precursor interleukin 1 beta (IL-1 beta) to an active IL-1 species by human mast cell chymase. *J Exp Med*. 1991;174(4):821–825.
43. Nakano A, Kishi F, Minami K, Wakabayashi H, Nakaya Y, Kido H. Selective conversion of big endothelins to tracheal smooth muscle-constricting 31-amino acid-length endothelins by chymase from human mast cells. *J Immunol*. 1997;159(4):1987–1992.
44. Zhao XY, et al. Chymase induces profibrotic response via transforming growth factor-beta 1/Smad activation in rat cardiac fibroblasts. *Mol Cell Biochem*. 2008;310(1-2):159–166.
45. Kofford MW, Schwartz LB, Schechter NM, Yager DR, Diegelmann RF, Graham MF. Cleavage of type I procollagen by human mast cell chymase initiates collagen fibril formation and generates a unique carboxyl-terminal propeptide. *J Biol Chem*. 1997;272(11):7127–7131.
46. Cianfrocca ME, et al. Phase 1 trial of the antiangiogenic peptide ATN-161 (Ac-PHSCN-NH(2)), a beta integrin antagonist, in patients with solid tumours. *Br J Cancer*. 2006;94(11):1621–1626.
47. Ricart AD, et al. Volociximab, a chimeric monoclonal antibody that specifically binds alpha-5beta1 integrin: a phase I, pharmacokinetic, and biological correlative study. *Clin Cancer Res*. 2008;14(23):7924–7929.
48. Kudo M, et al. Mfge8 suppresses airway hyperresponsiveness in asthma by regulating smooth muscle contraction. *Proc Natl Acad Sci U S A*. 2013;110(2):660–665.
49. Dougherty RH, et al. Accumulation of intraepithelial mast cells with a unique protease phenotype in T(H)2-high asthma. *J Allergy Clin Immunol*. 2010;125(5):1046–1053.e8.
50. Chen C, et al. Integrin α9β1 in airway smooth muscle suppresses exaggerated airway narrowing. *J Clin Invest*. 2012;122(8):2916–2927.
51. Kudo M, et al. IL-17A produced by αβ T cells drives airway hyper-responsiveness in mice and enhances mouse and human airway smooth muscle contraction. *Nat Med*. 2012;18(4):547–554.